

## Nanostructural features of demosponge biosilica

James C. Weaver,<sup>a,1</sup> Lía I. Pietrasanta,<sup>b,1</sup> Niklas Hedin,<sup>c,1</sup> Bradley F. Chmelka,<sup>c</sup>  
Paul K. Hansma,<sup>b</sup> and Daniel E. Morse<sup>a,\*</sup>

<sup>a</sup> Department of Molecular, Cellular, and Developmental Biology, University of California, Santa Barbara, CA 93106, USA

<sup>b</sup> Department of Physics, University of California, Santa Barbara, CA 93106, USA

<sup>c</sup> Department of Chemical Engineering, and the Materials Research Laboratory, University of California, Santa Barbara, CA 93106, USA

Received 8 April 2003, and in revised form 17 September 2003

### Abstract

Recent interest in the optical and mechanical properties of silica structures made by living sponges, and the possibility of harnessing these mechanisms for the synthesis of advanced materials and devices, motivate our investigation of the nanoscale structure of these remarkable biomaterials. Scanning electron and atomic force microscopic (SEM and AFM) analyses of the annular substructure of demosponge biosilica spicules reveals that the deposited material is nanoparticulate, with a mean particle diameter of  $74 \pm 13$  nm. The nanoparticles are deposited in alternating layers with characteristic etchant reactivities. Further analyses of longitudinally fractured spicules indicate that each deposited layer is approximately monoparticulate in thickness and exhibits extensive long range ordering, revealing an unanticipated level of nanoscale structural complexity. NMR data obtained from differentially heated spicule samples suggest that the etch sensitivity exhibited by these annular domains may be related to variation in the degree of silica condensation, rather than variability in the inclusion of organics. In addition, AFM phase imaging in conjunction with results obtained from HF and alkaline etching experiments suggest that at various stages in spicule biosynthesis, regions of unusually low silica condensation are deposited, indicating a possible interruption in normal spicule formation. While this discovery of nanoparticulate silica aggregation in demosponge skeletal elements is likely to reflect the intrinsic kinetic tendency of silica to form such particles during polycondensation, the hierarchical organization of these nanoparticles is biologically unique. © 2003 Elsevier Inc. All rights reserved.

**Keywords:** Porifera; *Tethya aurantia*; Spicules; Silicatein; Silicon; Biomineralization; Biomimetic

### 1. Introduction

The emerging field of silicon biotechnology has centered on understanding the mechanisms controlling biosilicification and its applications to the in vitro development of low-temperature routes to highly ordered silicon-based materials synthesis (Brott et al., 2001; Morse, 1999, 2001). Additional interest in the silica structures made by sponges has been stimulated by the recent characterization of the superior optical and interesting mechanical properties of these materials (Levi et al., 1989; Sarikaya et al., 2001; Sundar et al., 2003). Similarly, the remarkably complex structures made by

diatoms, a class of unicellular algae, have led to suggestions that these also might be used for technological applications (Parkinson and Gordon, 1999; Sandhage et al., 2002; Vrieling et al., 1999). Due to the complex nature of biosilicification, development of a tractable model system is essential if one is to understand the fundamentals of the underlying complex and dynamic biological processes. While previous research in this field has focused on structural analyses of diatom frustules (Hecky et al., 1973; Kröger et al., 1999, 2000; Lobel et al., 1996), and plant phytoliths (Carnelli et al., 2001; Theunissen, 1994), we have concentrated our efforts on biosynthetic skeletogenesis in siliceous demossponges (Porifera) (Garrone et al., 1981; Jones, 1979; Simpson et al., 1974, 1984, 1985; Uriz et al., 2000). In demossponges, skeletal support is often provided by highly ordered siliceous structures ranging in morphology from long needle-like strongyles to articulated, interdigitated

\* Corresponding author. Fax: 1-805-893-8062.

E-mail address: [d\\_morse@lifesci.ucsb.edu](mailto:d_morse@lifesci.ucsb.edu) (D.E. Morse).

<sup>1</sup> These authors contributed equally to this work.

fused networks of hypersilicified desmas as in the lithistid sponges, *Racodiscula* sp. (Hartman, 1981) and *Discodermia* sp. (Weaver and Morse, 2003) The supporting mineralized skeleton of *Tethya aurantia*, a common marine demosponge, is dominated by siliceous spicules (strongyloxea) measuring approximately 2 mm in length and 30  $\mu$ m in diameter (Fig. 1) which comprise ca. 75% of the dry weight of this organism (Shimizu et al., 1998). The large quantities of material available make this species a uniquely tractable model system for investigating the mechanisms of biosilicification. An additional advantage of this species is that unlike many other demosponges, *T. aurantia* lacks extensive intraspecific morphological variability, making species identification non-problematic. These attributes, coupled with its ease of culture under laboratory conditions, make *T. aurantia* a useful research subject.

Interest in sponge biosilicification is not a new field, but rather dates back to the early 1800s when it was first demonstrated that demosponge spicules are siliceous (Minchin, 1909). From fracture studies, these early investigations concluded that these spicules are composed of concentric lamellae (Bütschli, 1901), with a central axial filament of HF-resistant material that blackens upon heating, suggesting the presence of organic con-

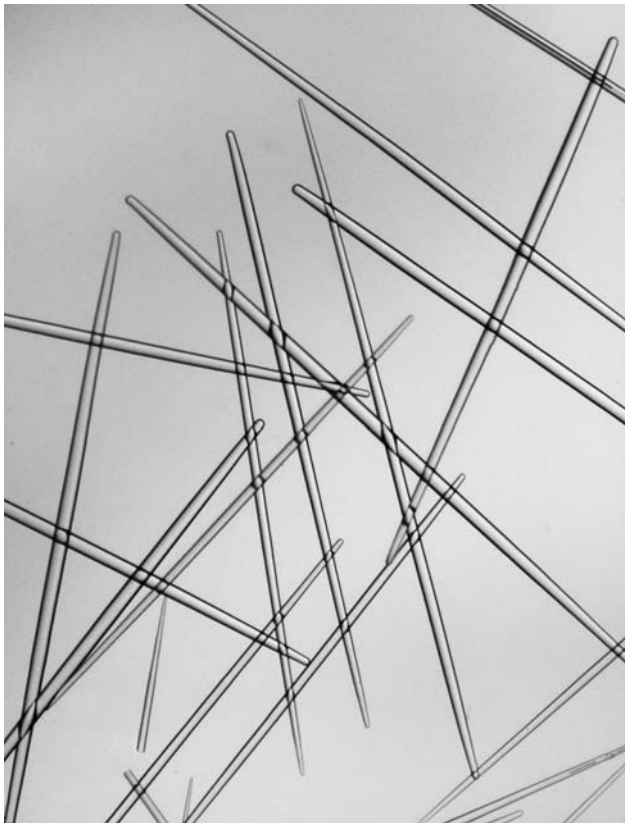


Fig. 1. Polarized light micrograph of strongyloxea (siliceous spicules) isolated from the temperate demosponge *T. aurantia*. Each spicule measures approximately 2 mm in length and 30  $\mu$ m in diameter.

stituents. More recently, it was demonstrated that this axial filament is proteinaceous (Shore, 1972) and has both templating as well as catalytic activity in directing the polymerization of silica and silsesquioxanes in vitro (Cha et al., 1999; Morse, 1999, 2000, 2001; Shimizu et al., 1998; Shimizu and Morse, 2000; Sumerel and Morse, 2003; Weaver and Morse, 2003; Zhou et al., 1999).

Although the untreated spicules of *T. aurantia* appear smooth, transparent, and glassy (Fig. 1), several observations prompted our more detailed investigation of their substructure: (1) investigations of the spicules of various demosponge taxa have revealed that they are composed of annular lamellae of silica (Bütschli, 1901; Schwab and Shore, 1971b; Simpson et al., 1985); (2) partial etching of spicules with HF revealed a nanoparticulate substructure (Cha, 2001); (3) the biosilicas made by diatoms (unicellular algae), revealed both by SEM (Schmid and Schulz, 1979; Volcani, 1981) and AFM (Noll et al., 2002; Wetherbee et al., 2000) analyses, exhibit a nanoparticulate substructure; and (4) silica formation in vitro mediated by diatom silaffins (Kröger et al., 1999, 2000) and by sponge spicule silicateins (Cha et al., 1999) is nanoparticulate. In fact, chemically synthesized silaffins have been used to guide the synthesis of an array of silica nanoparticles that functioned as a photonic crystal (Brott et al., 2001).

Schwab and Shore (1971a,b) observed conspicuous rings and concentric striations upon etching transverse spicule sections with HF. Their observations that prior heating of the biosilica prevented the appearance of etch-rings, in conjunction with their thermogravimetric analyses, led them to conclude that the etch-sensitive rings represented regions of less condensed (and thus, more hydrated) silica.

When observed by scanning electron microscopy, however, the superficial morphology appears highly consistent across the entire fractured spicule (Fig. 2A), without any indication of the annular deposits (Fig. 2B) that are revealed by HF etching. This supports the idea that the rings are due to relatively subtle compositional differences. The presence of zones of secondarily modified, but structurally similar material such as differentially dehydrated (i.e., condensed) silica, is one possible explanation, since variability in the degree of silica condensation could affect rates of etching by HF.

Until recently, however, technological limitations have been a major obstacle in further elucidation of the concentric siliceous substructure of demosponge spicules. This work builds on the pioneering AFM imaging done in 1998 (Egerton-Warburton et al., 1998) by providing new insights into the nanoscale ultrastructure of the deposited silica. Recently it was reported that formation of the terminal bulb during tylostyle maturation in the boring demosponges *Cliona tinctoria* and *Pione caesia* results from the secondary deposition of granular silica at one end of these linear spicules

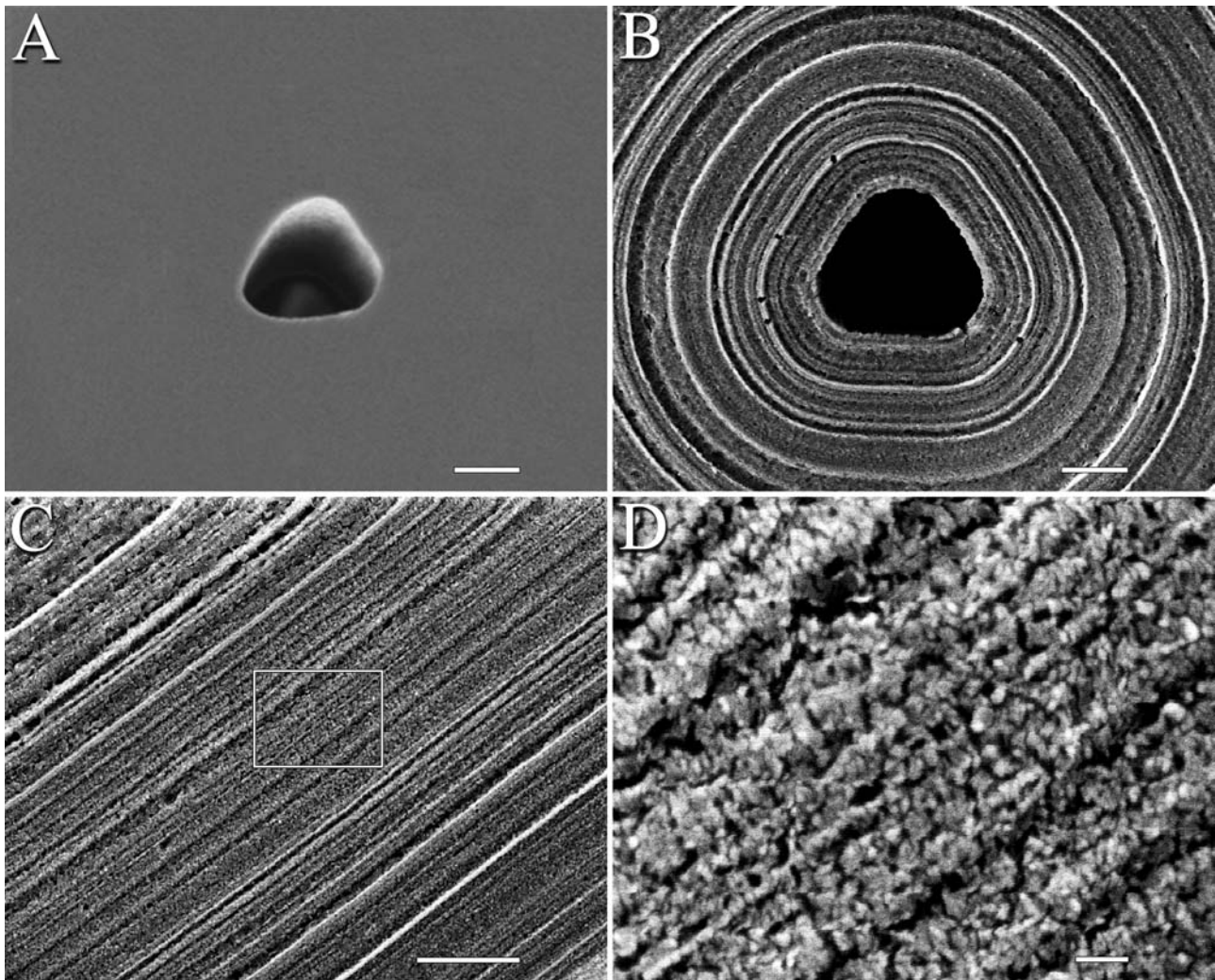


Fig. 2. (A) Scanning electron micrographs of freshly cleaved spicules from *T. aurantia*. (A) Scanning electron micrograph of an un-etched spicule cross section. The axial filament has been removed leaving a hollow central hexagonal cavity. (Scale bar: 1  $\mu\text{m}$ .) (B and C) Sodium hypochlorite-etched cross-section (B) and longitudinal-section (C) reveal concentric organization of the deposited silica. (Scale bars: 1  $\mu\text{m}$ .) (D) High-magnification (80 000 $\times$ ) scanning electron micrograph of boxed region in (C), revealing the nanoparticulate nature of the deposited silica. (Scale bar: 100 nm.)

(Schonberg, 2001). These results, however, did not reveal the gross silica nanostructuring of the spicule itself, as these observations were principally interpreted as a secondary spicule modification mechanism. Here, we report the use of high-resolution SEM in conjunction with AFM techniques to analyze the annular substructure of the siliceous spicules from the temperate demosponge *T. aurantia*. In conjunction with results obtained from NMR analyses of spicule samples heated to different temperatures, these observations relate for the first time the nanoparticulate substructure, the annular organization, and the differential etchant reactivity reported in independent analyses of demosponge biosilica, thus revealing an unanticipated level of structural complexity characteristic of these unique skeletal elements.

## 2. Materials and methods

### 2.1. Isolation of spicules

Specimens of the marine sponge *T. aurantia* were collected at 17 m depths off Santa Barbara County, California (latitude 34°25.331'N, longitude 119°57.142'W) in July, 2000. Sponges were washed with seawater and treated with a 5.25% (v/v) sodium hypochlorite solution until all of the cellular material had been removed. The residual material was washed with Milli-Q (Millipore)-purified water five times and then soaked in concentrated  $\text{HNO}_3/\text{H}_2\text{SO}_4$  (1:4) overnight. Acid-insoluble material (which consisted entirely of the cleaned silica spicules) was rinsed with Milli-Q water until the pH was  $\geq 6$ , and then air-dried. Fig. 1

illustrates the cleaned spicules utilized for the following experiments.

## 2.2. Preparation of spicules for microscopy

Similar preparative techniques were used for both SEM and AFM analyses. After drying, the spicules were ground with a mortar and pestle until greater than 75% of the fragments were of the appropriate size for microscopic analyses. After fracture, the spicule fragments were rinsed with Milli-Q water, the suspension allowed to settle, and the fine particulates remaining in the suspension were decanted and discarded. The duration of time for gravity settling and the number of washings performed varied as a function of grinding intensity and the desired size of the final fragments to be examined. To avoid potential imaging artifacts resulting from the use of mounting adhesives, none were used for the following studies. The spicule fragments were resuspended in 95% ethanol and small volumes were pipetted onto 12 mm round glass cover-slips (Fisherbrand, Pittsburgh, PA), the samples were air-dried, and examined microscopically. Adhesion to the glass cover-slips was facilitated entirely by electrostatic and/or other adhesive forces between the spicule fragments and the glass substrates. As specified, some samples were etched by treatment with sodium hypochlorite (5.25% v/v) for 6 weeks, washed five times with Milli-Q water and three times with 95% ethanol, and mounted for examination as described above.

## 2.3. Electron microscopy

The dried spicules (mounted on 12 mm round glass cover-slips) were sputter coated with gold/palladium and observed with a JEOL JSM 6300F cold-cathode field-emission scanning electron microscope.

## 2.4. Atomic force microscopy

All imaging was performed with a Dimension 3100 SPM (Digital Instruments, Santa Barbara, CA) equipped with commercially available silicon cantilevers (nominal tip radius of 10 nm) measuring 125  $\mu\text{m}$  in length. The cantilever oscillation frequency was tuned to the resonant frequency of the cantilever (280–350 kHz) and all imaging was performed in air at ambient conditions. The 512  $\times$  512 pixel images were captured with a scan size between 0.6 and 10  $\mu\text{m}$  at a scan rate of 0.5–2 lines per second. Images were acquired simultaneously from the height, amplitude, and phase signals. All imaging was done in tapping mode to minimize sample damage and to reduce the probability of dislodging the spicule fragments during scanning. Images were further processed by flattening using Nanoscope Software (Digital Instruments) to remove background slope.

## 2.5. Treatments with HF and heat

Freshly cleaved spicule cross-sections were analyzed for heat-induced structural changes to the deposited silica. (1) Spicule cross-sections were etched with 1 M HF for 1 min [an excellent technique for rapid visualization of the annular silica organization (Schwab and Shore, 1971b)], washed five times with Milli-Q water and three times with 95% ethanol, and air-dried. The samples then were heated (in air) to 300 and 600  $^{\circ}\text{C}$  for 1 h and any heat-induced structural changes were analyzed by SEM. (2) As a control, additional spicule cross sections were first heated to 300 and 600  $^{\circ}\text{C}$  for 1 hour and then treated with 1 M HF for 1 min, washed and dried as described above. Any effect that the prior heating had on the samples' reactivity to HF treatment was analyzed by SEM. Samples were mounted for examination as described above. The heated samples (and a non-heat-treated control) also were analyzed by NMR spectroscopy.

## 2.6. NMR analyses

Solid-state  $^{29}\text{Si}$  NMR spectra were acquired in a temperature-controlled room (20–23  $^{\circ}\text{C}$ ) on a Chemagnetics CMX-500 spectrometer using an 11.7 T wide bore magnet. A double resonance magic-angle-spinning (MAS) probehead with no  $^{29}\text{Si}$  background signal was used with 7.5 mm Pencil MAS rotors containing 400–500 mg of powdered sample. The  $^{29}\text{Si}$  MAS NMR spectra were acquired with samples spinning at a rate of 6 kHz using an 8.6  $\mu\text{s}$  90 $^{\circ}$  pulse and a continuous  $^1\text{H}$ -decoupling field strength of  $\nu_{\text{dec}} = 12.5$  kHz. A spectral width of 16 kHz was used during signal acquisition, with a filter width of 10.4 kHz; 256 time domain points were acquired for each transient. Gaussian filtering of 100 Hz (which is small compared to the  $^{29}\text{Si}$  NMR peak widths) was applied during data processing. The  $^{29}\text{Si}$  chemical shift scale was externally calibrated to the known chemical shifts of tetrakis(trimethylsilyl)silane [–9.8 ppm for the  $\text{CH}_3\text{-Si-}$  groups referenced to the chemical shift standard tetramethylsilane (TMS)]. Three samples were investigated by  $^{29}\text{Si}$  MAS NMR: a non-heated control sample (A), one heated to 300  $^{\circ}\text{C}$  (B), and one heated to 600  $^{\circ}\text{C}$  (C) (see *Heat Treatment* section for details). Recycle times between successive signal acquisitions were 10 min for samples A and B and 260 min for sample C. The recycle times were chosen to prevent saturation of any parts of the spectrum during prolonged signal averaging. These differences show that the  $^{29}\text{Si}$   $T_1$  relaxation times for sample (C) are approximately an order of magnitude larger than for samples (A) and (B).  $T_1$  relaxation times are measures of the rates at which the longitudinal component of the nuclear magnetization is restored to thermal equilibrium. More transients were acquired for sample (B) than for sample

(A) to improve the signal-to-noise ratio and thereby elucidate the less resolved features at larger chemical shifts in the  $^{29}\text{Si}$  spectrum of (B).

A two dimensional  $^{29}\text{Si}\{^1\text{H}\}$  heteronuclear correlation NMR spectrum (Janicke et al., 1998; Schmidt-Rohr and Spiess, 1994) was acquired for the non-heated sample (A) under MAS conditions at a spinning rate of 6 kHz. A  $^1\text{H}$  spin-diffusion delay (Goldman and Shen, 1966) of 75 ms was included in the pulse sequence to allow resonance signals from spatially proximate moieties to be correlated up to distances of ca. 20 nm (Schmidt-Rohr and Spiess, 1994). The contact time of 4 ms for the *rf* field-driven cross polarization from  $^1\text{H}$  to  $^{29}\text{Si}$  was optimized by maximizing the  $^{29}\text{Si}$  NMR signal intensity for the  $Q^3$  silica species. Using time-proportional phase increments enabled an in-phase spectrum to be acquired. A continuous  $^1\text{H}$ -decoupling field strength of  $\nu_{\text{dec}} = 25$  kHz was applied during detection of the  $^{29}\text{Si}$  NMR transients with a spectral width of 25 kHz and a filter width of 16 kHz. Each  $^{29}\text{Si}$  NMR transient consisted of 256 time domain points, and 256 transients were acquired for each increment in the  $^1\text{H}$  NMR time-domain with a recycle delay of 4 s. Fifty-nine  $^1\text{H}$  NMR transients were detected indirectly with a spectral width of 10 kHz; a Gaussian filter of 100 Hz was applied to the  $^{29}\text{Si}$  NMR time-domain and a sine-bell filter to the  $^1\text{H}$  NMR time-domain before 2D Fourier transformation. The  $^{29}\text{Si}$  and the  $^1\text{H}$  chemical shift scales were externally calibrated to the known chemical shifts of tetra-kis(trimethylsilyl)silane.

### 3. Results

#### 3.1. SEM analyses of fractured spicules

Investigation of the morphology of freshly cleaved spicule cross-sections by SEM revealed no detectable concentric organization of the deposited silica. In many instances, the axial protein filament was found dislodged, leaving the central hexagonal axial channel empty (Fig. 2A). The interior of this channel often exhibited nanoparticulate surface features, while the fractured silica did not. Annular substructure in the spicule cross-sections became apparent only after long-term alkaline or brief HF etching (Figs. 2B and 5). Regions subsequently identified as containing less condensed (more hydrated) siliceous material etched at a faster rate relative to those containing more highly condensed silica (Figs. 2B and 5). High-magnification imaging of sodium hypochlorite-treated longitudinal sections (Figs. 2C and D) reveals long-range ordering of the deposited silica nanoparticles. Similar results were obtained with other alkaline etchants such as NaOH (data not shown) or brief 1 M HF treatments, although, due to the rapid rate of HF-demineralization, nanostructural details of the

annular substructure were frequently obscured by extensive surface roughening caused by the HF.

#### 3.2. AFM analyses of fractured spicules

Although undetectable with high-resolution SEM imaging, AFM analyses revealed the presence of nanoparticulate silica organized around the central axial filament of freshly cleaved (un-etched) spicule cross-sections (Fig. 3A). The sizes of these particles are consistent with the data obtained from the sodium hypochlorite-treated SEM images (Fig. 2D), revealing a mean particle diameter of  $74 \pm 13$  nm ( $n = 75$ ); the concentric organization of these particles is clearly evident (Figs. 3A and B). AFM phase imaging also revealed the presence of relatively rare annular regions that exhibit both higher topography and phase contrast (Figs. 3B and C). After treatment of fractured spicules with sodium hypochlorite, NaOH, or HF, AFM analyses revealed increased prominence of the annular substructure as the more hydrated regions (cf. below) are etched more quickly. Although the depth of the valleys between successive etch-resistant rings increased with sequential etching (Figs. 4A and B), there was negligible reduction in mean particle diameter of this more condensed (and thus more etch-resistant) material (standard deviation  $\geq$  magnitude of average difference before and after etching). High-magnification analysis (Fig. 4C)—with a scan size of  $2 \mu\text{m}$ —of longitudinally cleaved sections indicates that each layer is approximately monoparticulate in thickness (Fig. 5A), revealing an unanticipated level of structural complexity of the deposited silica. While the annular structuring of this material has been known from previous work, these studies reveal for the first time that these annuli are deposited with nanoscale regularity across macroscopic length scales.

#### 3.3. Treatments with HF and heat

Heating spicule cross-sections to  $300^\circ\text{C}$  for one hour appeared to have a negligible effect on both the etchant reactivities and the annular morphologies of samples etched prior to heating. When similar samples were heated to  $600^\circ\text{C}$  for 1 h, however, this dramatically altered the subsequent etchant reactivities, as no annular features could be observed upon HF treatment after heating to this temperature. Interestingly, however, there did not appear to be significant morphological alteration to the HF-revealed annular features after heating to  $600^\circ\text{C}$  for previously etched samples (data not shown).

In addition to the standard etch rings that appear following exposure to HF, there also were annular regions that exhibited unusually high-etch sensitivity. The abundance of these regions varied dramatically from spicule to spicule, from undetectable to several per specimen examined. The spicule cross-section shown in

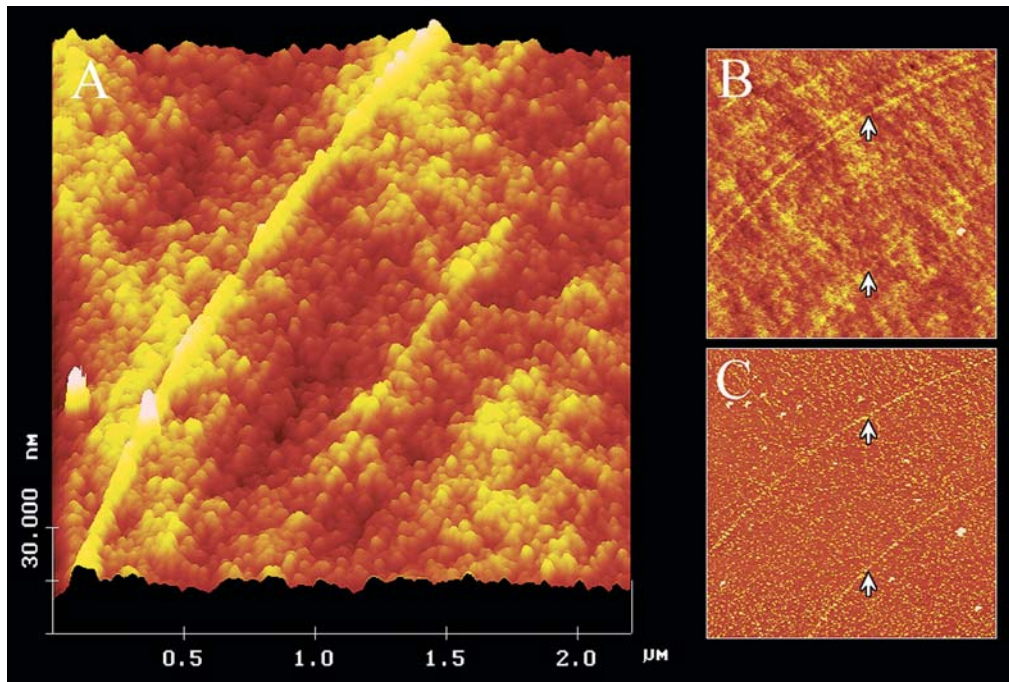


Fig. 3. (A) AFM surface plot of a freshly cleaved (un-etched) spicule cross-section revealing the existence of concentric arrays of nanoparticulate silica. (B) Top view and (C) phase mode image of the same preparation. Note the relatively rare rings of higher phase-contrast, as shown by the white arrows (cf Fig. 5). Scan sizes: 2.25 μm.

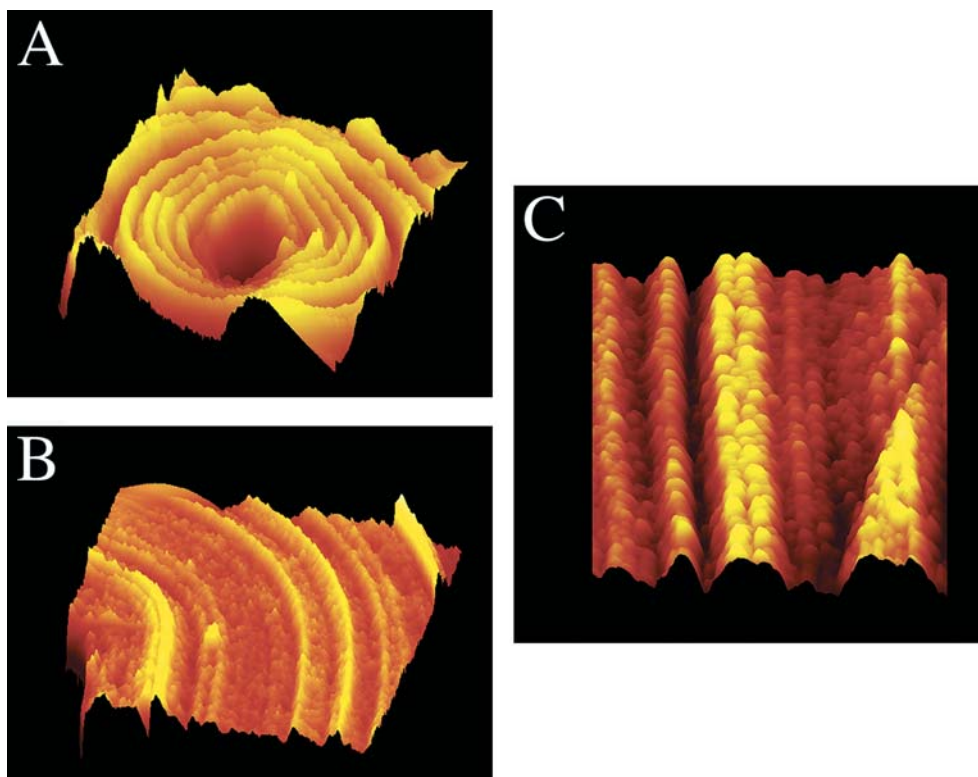


Fig. 4. AFM surface plots of sodium hypochlorite-treated (etched) spicule cross sections (A and B) and longitudinal-section (C). (A) Illustrates concentric organization of deposited silica, while (B and C) reveal the annular nanoparticulate substructure. (A) Scan size 10 μm, z data scale 250 nm; (B) scan size 3.8 μm, z data scale 275 nm; (C) scan size 2 μm, z data scale 75 nm.

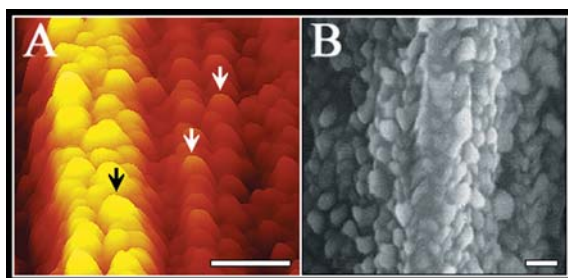


Fig. 5. (A) AFM surface plot of spicule longitudinal section (enlargement of a portion of Fig. 4C) revealing annular organization of the deposited silica. Scale bar: 250 nm. The arrows indicate individual layers that are nearly monolayer in thickness. (B) Scanning electron micrograph illustrating nanoparticulate silica visible after brief treatment of intact spicules with HF. Scale bar: 100 nm.

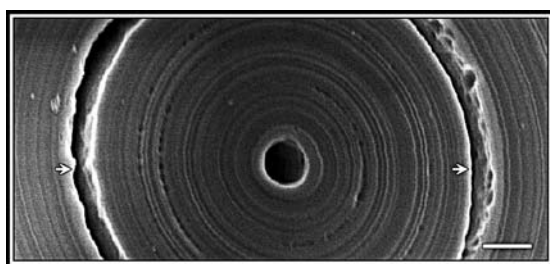


Fig. 6. Scanning electron micrograph of HF-treated spicule cross section revealing regions of differential etchant reactivities. The arrows indicate an uncommon zone that etches at a considerably faster rate compared to that of the surrounding material. This region may correspond to the rings of high-AFM phase-contrast shown in Fig. 3C and could represent a zone of poorly condensed (highly hydrated) silica, which are known to etch at faster rates than more condensed material. Scale bar = 1  $\mu$ m.

Fig. 6 exhibits one of these regions (indicated by the arrows).

### 3.4. NMR analyses

Single-pulse  $^{29}\text{Si}$  MAS NMR spectra of siliceous spicules isolated from *T. aurantia* heated to 300 and 600  $^{\circ}\text{C}$  are shown in Fig. 7, revealing different degrees of heat-induced silica condensation. The results show that the inorganic silica framework is moderately condensed, even in the non-heat-treated sample. The chemical shift of the dominant peak at  $-112$  ppm in Fig. 7A corresponds to  $Q^4$  silica units,<sup>2</sup> and the less intense peak at  $-101$  ppm corresponds to  $Q^3$  moieties (Engelhardt and Michel, 1987). By deconvoluting the spectra in Figs. 7A and B into two Gaussian spectral lines, the  $Q^4 : Q^3$  ratios are estimated to be 3:1 in both the non-heat-treated sample (A) and sample (B) heated to 300  $^{\circ}\text{C}$ . The left shoulder and the asymmetry of the peak at  $-112$  ppm in Fig. 7B reveal that  $Q^3$  moieties are still present, while the

<sup>2</sup> In this notation,  $Q^n$  refers to tetrahedrally coordinated silicon atoms,  $Q$ , having  $n$  neighboring  $-\text{O}-\text{Si}$ -groups.

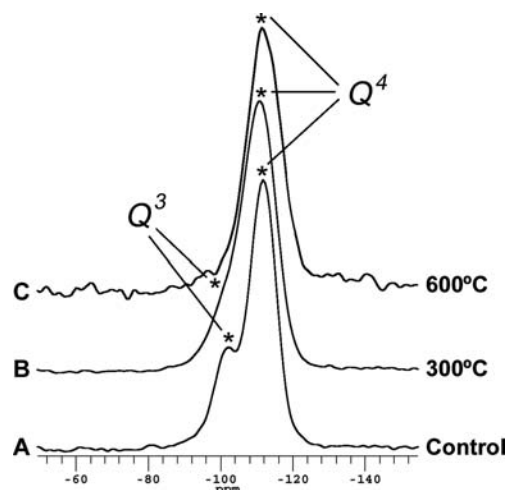


Fig. 7. Single-pulse magic-angle-spinning  $^{29}\text{Si}$  NMR spectra of siliceous spicules isolated from *T. aurantia* heated to 300 and 600  $^{\circ}\text{C}$ , revealing the degree of heat-induced silica condensation. Spectrum (A) is from non-heat-treated spicules, (B) from spicules heated to 300  $^{\circ}\text{C}$  and (C) from spicules heated to 600  $^{\circ}\text{C}$ . The peak at  $-102$  ppm in (A) and the shoulder of the peak at  $-112$  ppm in (B) correspond to incompletely condensed  $Q^3$  silica moieties ( $Q^3/Q^4$  is ca. 0.3–0.4 for samples A and B). The larger integral area of the peak at  $-112$  ppm shows that fully condensed ( $Q^4$ ) silica groups are more abundant than  $Q^3$  species. In (C), there is no evidence of a significant fraction of  $Q^3$  moieties remaining ( $Q^3/Q^4 < 0.1$ ).

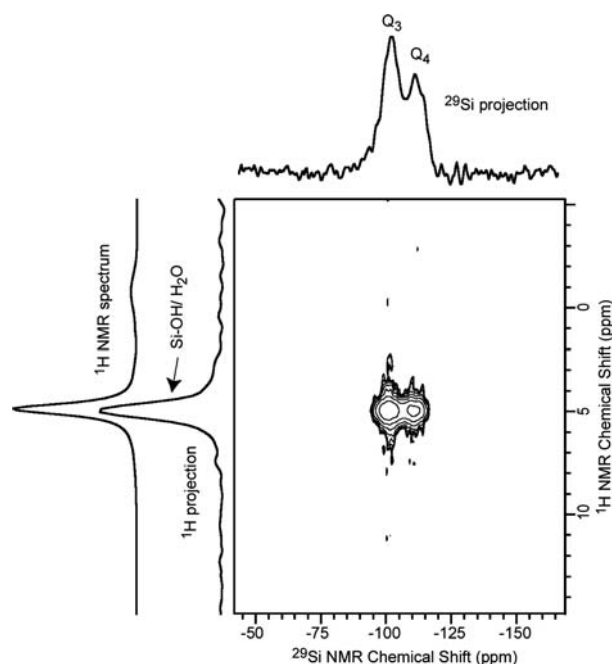


Fig. 8. A 2D  $^{29}\text{Si}\{^1\text{H}\}$  heteronuclear correlation NMR spectrum of the non-heat-treated siliceous spicules, with accompanying projections of the intensities in the contour plot and a single-pulse  $^1\text{H}$  NMR spectrum. There are strong intensity correlations between the silica  $Q^3$  and  $Q^4$  moieties with  $\text{Si}-\text{OH}$  or adsorbed water at their typical  $^1\text{H}$  NMR chemical shift value of ca. 5 ppm. No evidence for molecular contact between the silica and organic matter was found. The dominant peak at ca. 5 ppm in the  $^1\text{H}$  NMR spectrum corroborates that overall small quantities of organic matter are present in the silica surrounding the spicules organic axial filament.

spectrum obtained from the sample heated to 600 °C shows no evidence of  $Q^3$  moieties remaining (Fig. 7C). These differences correlate with differences in  $^{29}\text{Si}$   $T_1$  relaxation times: the samples with appreciable  $Q^3$  species (A and B) have substantially shorter  $T_1$  values than sample (C), which is comprised almost exclusively of  $Q^4$  moieties; an upper limit of the  $Q^3 : Q^4$  ratio  $<0.1$  was estimated by deconvolving the spectrum in Fig. 7C into two Gaussian spectral components. Under otherwise identical conditions, the narrower linewidth of the  $Q^4$  peak in Fig. 7A (approximately 70% of that in Figs. 7B and C) reflects the more homogeneous environments of the fully polymerized (condensed) silica sites in the non-heat-treated sample (A), compared to those in heat-treated samples (B) and (C). This indicates that the heat-induced transformation of  $Q^3$  into  $Q^4$  groups broadens the distribution of Si–O–Si bond angles and distances.<sup>3</sup>

A 2D  $^{29}\text{Si}\{^1\text{H}\}$  heteronuclear correlation NMR spectrum of non-heat-treated siliceous spicules is shown in Fig. 8. Two strong intensity correlations are evident between the  $Q^3$  and  $Q^4$   $^{29}\text{Si}$  chemical shifts<sup>4</sup> and one  $^1\text{H}$  chemical shift. The  $^1\text{H}$  chemical shift at ca. 5 ppm is assigned to Si–OH groups or adsorbed  $\text{H}_2\text{O}$  according to their chemical shift values (Engelhardt and Michel, 1987). The single-pulse  $^1\text{H}$  MAS NMR spectrum in Fig. 8 has two spectral lines, one intense at ca. 5 ppm from Si–OH or adsorbed water and one weaker at around –1 ppm. These results indicate that the silica moieties are not in molecular proximity to detectable quantities of organic species.

#### 4. Discussion

The process of biosilicification has presumably evolved independently in a wide range of phylogenetically diverse taxa with representatives ranging from diatoms and radiolaria to sponges and higher plants (Simpson and Volcani, 1981). The convergent nature of this mineralizational motif is clearly evident from the unique taxa-specific biomolecules that are occluded in the condensed products (Kröger et al., 1999, 2000; Shimizu et al., 1998). A common theme that many of these groups employ in the polymerization of silica is that the polycondensed product is nanoparticulate in nature (Cha et al., 1999; Noll et al., 2002; Schmid and Schulz, 1979; Volcani, 1981; Wetherbee et al., 2000). This is not

surprising, since the polycondensation of silica in aqueous media is kinetically driven to form such particles, which then aggregate and condense via their surface hydroxyls (Iler, 1979).

In frustules of the diatom, *Cylindrotheca fusiformis*, for example, the polycationic silaffins (named for their affinity for silica), which are occluded within the frustule silica, are extensively post-translationally modified with polyamine and phosphate functionalities to specific amino acid sidechains (Kröger et al., 1999, 2002). When added to metastable silicic acid, these peptides induce the rapid polycondensation and synthesis of silica nanospheres with fairly uniform morphologies. In addition to the species-specific silaffins occluded with the frustules of diatoms, high amounts of free (non-peptide linked) long-chain polyamines also are occluded (Kröger et al., 2000). These polyamines also promote the precipitation of silica in vitro, and the resulting condensed silica spheres exhibit polyamine-specific size dependencies. It is currently thought that the cooperative interactions of these longchain polyamines and the silaffins, in conjunction with phase-separation, may be responsible for mediating the formation of the species-specific nanoscale frustule morphologies observed in vivo (Kröger et al., 2000; Sumper, 2002). Significantly, the sizes of the silica nanoparticles produced by the silaffins and polyamines in vitro are similar to those revealed by AFM in native diatom frustules (Crawford et al., 2001; Noll et al., 2002; Wetherbee et al., 2000).

Although it had been previously reported that HF etched demosponge spicules revealed a nanoparticulate substructure (Fig. 5B), these experiments did not reveal hierarchical, annular ordering of the particles (Cha, 2001). The results reported here reveal the nanostructural architecture of this material and illustrate the precise, hierarchical control that is exhibited over mineral deposition during demosponge spicule formation.

The different etchant reactivities exhibited by this biosilica in conjunction with our microscopic and NMR analyses before and after high-temperature (600 °C) induced condensation support the suggestion (Schwab and Shore, 1971b) that the annular pattern reflects differences in the extent of silica condensation during deposition, rather than the inclusion of appreciable quantities of organic material. The observation that the SEM-detectable annular substructure of previously HF-etched samples was not significantly altered upon heating to 600 °C indicates that the duration of heating was not sufficient for temperature-induced melting of the deposited silica. Together with the NMR results, this supports the proposal that heating to 600 °C results in almost complete silica condensation (accompanied by a loss in etch sensitivity) and is not an organic degradation or silica mobilization (melting) process. This is confirmed by the disappearance of the  $Q^3$  NMR species and the substantial increase in the  $T_1$  relaxation parameter,

<sup>3</sup> Other possible contributions to these differences can effectively be ruled out. The magnitude of the field inhomogeneity is on the order of 20 Hz, and homogenous linewidths are expected to be less than 1 Hz for  $^{29}\text{Si}$   $Q^4$  moieties in natural abundance in purely siliceous materials (Anderson, 1992).

<sup>4</sup> Note that the  $^{29}\text{Si}$  projection of Fig. 8 is quite different from Fig. 7A. This is a result of the  $^{29}\text{Si}\{^1\text{H}\}$  heteronuclear NMR measurement conditions were optimized to be more sensitive to  $Q^3$  moieties.

corroborating a dramatic decrease in the abundance of silanol groups. If large quantities of organic material had been initially incorporated within the deposited silica (e.g., between the annular layers), then at sub-mobilization temperatures, one might expect to see concentric banding or pitting appear after heating-induced destruction of organics, which in these experiments was not observed. The  $^1\text{H}$  NMR spectrum of the non-heat-treated spicules (Fig. 8) shows no signals in the range of 1–2 ppm that are characteristic of aliphatic organic species. The 2D  $^{29}\text{Si}\{^1\text{H}\}$  NMR spectrum (Fig. 8) establishes that only signals from Si–OH (or adsorbed water) and the silica framework are strongly correlated and thus in close molecular proximity. The dominance of the Si–OH and water  $^1\text{H}$  NMR signals is consistent with our proposal that there exist negligible quantities of organic material in intimate association with the silica nanoparticles that surround the spicule axial filament; such organic matter thus could not feasibly contribute appreciably to the observed dramatic difference in etchant reactivity of the silica annuli.

Results from HF- or alkaline-etching experiments reveal the existence of sparsely distributed annular siliceous deposits with unusually high-etchant reactivities (Fig. 6). These localities could represent regions of poorly condensed (highly hydrated) silica and may indicate abnormal variability in silica deposition during spicule biosynthesis. This suggestion is supported by the relative rarity of these regions within an individual spicule, and by the high degree of spatial variability exhibited from spicule to spicule (in which these low density regions vary in abundance from undetectable to several per specimen examined). Interestingly, the relative rarity of these regions roughly corresponds to the abundance of annuli of high-AFM phase-contrast, such as those shown in Fig. 3C. While at least some of this observed contrast could be explained by topographical differences, there are potentially other contributing factors, such as slight compositional differences in the material being examined, that should be considered. Based on these observations, we cannot rule out the possibility that there may exist a correspondence between these high-AFM phase-contrast regions and those of very high-etch sensitivity, such as shown in Fig. 5.

It should be noted that the paucity of organic material in direct association with the silica annuli surrounding the axial filament in demosponges such as *Tethya* differs markedly from the structure of spicules isolated from hexactinellid sponges (Sundar et al., 2003). This difference also can be expected to result in significant differences in the mechanical and fracture properties of the spicules of these two very different groups of sponges, the Demospongiae and the Hexactinellida (Levi et al., 1989; Sarikaya et al., 2001).

One remaining paradox in understanding demo-sponge spicule biosynthesis is the mechanism by which

silica deposition continues once the proteinaceous axial filament has become completely covered during the early stages of spicule formation. The polymerization-promoting activity of the silicateins (that comprise >98% of the central axial filament in the *Tethya* spicules; cf. Shimizu et al., 1998) has been shown to be catalytic and not stoichiometric. Our observations and previous reports indicate that this catalytic activity is retained by the individual subunits liberated after axial filament solubilization (Cha et al., 1999) as well as those synthesized from recombinant DNA templates (Zhou et al., 1999; Zhou, Cao, Sumerel, and Morse, unpublished observations). It is possible that the controlled punctuated secretion of low concentrations of monomeric silicateins, pulses in the transitory flux of silica-precursor molecules, oscillations in the pH, ionic or other conditions of the condensation environment, or a combination of these factors may be responsible for the annular patterning and continued deposition of silica in spicule biosynthesis in vivo once the axial filament has become completely covered during the early stages of silica deposition around this proteinaceous core. Alternatively, the continued growth of silica may be a result of dangling bonds at the growth surface of the newly deposited silica (Saito et al., 1995).

Based on the dramatically different mechanisms of biosilicification in demosponges and diatoms—apparently mediated, at least initially, by insoluble filamentous catalytic protein scaffolds in demosponges and monomeric, stoichiometric polyamines in diatom frustules—it is likely that the similar nanoparticulate structural motifs of the deposited silica are a consequence of the intrinsic colloidal behavior of silica during polycondensation from aqueous media (Iler, 1979). The stoichiometric activity of the diatom silafins involved in silica polymerization (Kröger et al., 1999, 2000) is fundamentally similar to the induction of silica polycondensation by synthetic polyamines (Mizutani et al., 1998), while the silicateins are both catalytic and structure-directing. Although the biomolecular components directing the condensation and assembly processes may differ, the kinetic drive to form nanoparticulates of silica is evident in these two very different systems.

## Acknowledgments

We thank J.N. Cha and M. Brzezinski for helpful suggestions, and L.J. Freisen for the light micrograph in Fig. 1 and J.N. Cha for the electron micrograph in Fig. 5. This work was supported by Grants from NASA (#NCC-1-02037), the US Army Research Office (#DAAD 19-001-0564), the NOAA National Sea Grant Program, US Department of Commerce, under Grant NA36RG0537, Project E/G-2, through the

California Sea Grant College System, and the MRSEC Program of the National Science Foundation under awards No. DMR-96-32716 and DMR-00-80034 to the UCSB Materials Research Laboratory. N.H. thanks the Swedish STINT foundation for support.

## References

- Anderson, M.W., 1992. Application of DEFT and SEFT for signal-to-noise ratio enhancement and  $T_2$ -selective spectra in  $^{29}\text{Si}$  MAS NMR of zeolites. *J. Magn. Reson. Chem.* 30, 898–904.
- Brott, L.L., Naik, R.R., Pikas, D.J., Kirkpatrick, S.M., Tomlin, D.W., Whitlock, P.W., Clarkson, S.J., Stone, M.O., 2001. Ultrafast holographic nanopatterning of biocatalytically formed silica. *Nature* 413, 291–293.
- Bütschli, O., 1901. Einige beobachtungen über kiesel- und kalknadeln von spongien. *Z. Wiss. Zool.* 69, 235–286.
- Carnelli, A.L., Madella, M., Theurillat, J.P., 2001. Biogenic silica production in selected alpine plant species and plant communities. *Ann. Bot.—London* 87, 425–434.
- Cha, J.N., Shimizu, K., Zhou, Y., Christiansen, S.C., Chmelka, B.F., Stucky, G.D., Morse, D.E., 1999. Silicatein filaments and subunits from a marine sponge direct the polymerization of silica and silicones in vitro. *Proc. Natl. Acad. Sci. USA* 96, 361–365.
- Cha, J.N., 2001. Lessons from nature: novel routes to biomimetic synthesis of silica based materials. Ph.D. Thesis, UCSB.
- Crawford, S.A., Higgins, M.J., Mulvaney, P., Wetherbee, R., 2001. Nanostructure of the diatom frustule as revealed by atomic force and scanning electron microscopy. *J. Phycol.* 37 (4), 543–554.
- Egerton-Warburton, L.M., Huntington, S.T., Mulvaney, P., Griffin, B.J., Wetherbee, R., 1998. A new technique for preparing biomaterials for atomic-force microscopy. *Protoplasma* 204, 34–37.
- Engelhardt, G., Michel, D., 1987. High-resolution solid-state NMR of silicates and zeolites. Wiley, Chichester.
- Garrone, R., Simpson, T.L., Pottu-Boumendil, J., 1981. Ultrastructure and deposition of silica in sponges. In: Simpson, T.L., Volcani, B.E. (Eds.), *Silicon and Siliceous Structures in Biological Systems*. Springer-Verlag, New York, pp. 495–525.
- Goldman, M., Shen, L., 1966. Spin-spin relaxation in  $\text{LaF}_3$ . *Phys. Rev.* 144, 321–331.
- Hartman, W.D., 1981. Form and distribution of silica in sponges. In: Simpson, T.L., Volcani, B.E. (Eds.), *Silicon and Siliceous Structures in Biological Systems*. Springer-Verlag, New York, pp. 453–493.
- Hecky, R.E., Mopper, K., Kilham, P., Degens, E.T., 1973. Amino-acid and sugar composition of diatom cell-walls. *Mar. Biol.* 19, 323–331.
- Iler, R.K., 1979. *The Chemistry of Silica; Solubility, Polymerization, Colloidal and Surface Properties, and Biochemistry*. John Wiley and Sons, New York.
- Janicke, M.T., Landry, C.C., Christiansen, S.C., Kumar, D., Stucky, G.D., Chmelka, B.F., 1998. Aluminum incorporation and interfacial structures in MCM-41 mesoporous molecular sieves. *J. Am. Chem. Soc.* 120, 6940–6951.
- Jones, C.W., 1979. The microstructure and genesis of sponge biomaterials. In: Lévi, C., Boury-esnault, N. (Eds.), *Biologie des Spongiaires. Colloques internat. C.N.R.S.* 291, 425–447.
- Kröger, N., Deuzmann, R., Sumper, M., 1999. Polycationic peptides from diatom biosilica that direct silica nanosphere formation. *Science* 286, 1129–1132.
- Kröger, N., Deuzmann, R., Bergsdorf, C., Sumper, M., 2000. Species-specific polyamines from diatoms control silica morphology. *Proc. Natl. Acad. Sci. USA* 97, 14133–14138.
- Kröger, N., Lorenz, S., Brunner, E., Sumper, M., 2002. Self-assembly of highly phosphorylated silaffins and their function in biosilica morphogenesis. *Science* 298, 584–586.
- Levi, C., Barton, J.L., Guillemet, C., Lebras, E., Lehuède, P., 1989. A remarkably strong natural glassy rod—the anchoring spicule of the *Monorhaphis* sponge. *J. Mater. Sci. Lett.* 8, 337–339.
- Lobel, K.D., West, J.K., Hench, L.L., 1996. Computational model for protein-mediated biomineralization of the diatom frustule. *Marine Biol.* 126, 353–360.
- Minchin, E.A., 1909. A summary of present knowledge. *Ergeb. Fortschr. Zool.* 2, 171–274.
- Mizutani, T., Nagase, H., Fujiwara, N., Ogoshi, H., 1998. Silicic acid polymerization catalyzed by amines and polyamines. *Bull. Chem. Soc. Jpn.* 71, 2017–2022.
- Morse, D.E., 1999. Silicon biotechnology: harnessing biological silica production to construct new materials. *Trends Biotechnol.* 17, 230–232.
- Morse, D.E., 2000. Silicon biotechnology: proteins, genes and molecular mechanisms controlling biosilica nanofabrication offer new routes to polysiloxane synthesis. In: Auner, N., Weis, J. (Eds.), *Organosilicon Chemistry IV: From Molecules to Materials*. Wiley-VCH, New York, pp. 5–16.
- Morse, D.E., 2001. Biotechnology reveals new routes to synthesis and structural control of silica and polysilsesquioxanes. In: Rappoport, Z., Apeloig, Y. (Eds.), *The Chemistry of Organic Silicon Compounds*, vol. 3. Wiley, New York, pp. 805–819.
- Noll, F., Sumper, M., Hampp, N., 2002. Nanostructure of diatom silica surfaces and of biomimetic analogues. *Nano Lett.* 2, 91–95.
- Parkinson, J., Gordon, R., 1999. Beyond micromachining: the potential of diatoms. *Trends Biotechnol.* 17 (5), 190–196.
- Saito, Y., Isobe, T., Senna, M., 1995. Incipient chemical reaction on the scratched silicon (111) surface with ethoxy and hydroxyl-groups. *J. Solid State Chem.* 120 (1), 96–100.
- Sarikaya, M., Fong, H., Sunderland, N., Flinn, B.D., Mayer, G., Mescher, A., Gaiino, E., 2001. Biomimetic model of a sponge-spicular optical fiber-mechanical properties and structure. *J. Mater. Res.* 16, 1420–1428.
- Sandhage, K.H., Dickerson, M.B., Huseman, P.M., Caranna, M.A., Clifton, J.D., Bull, T.A., Heibel, T.J., Overton, W.R., Schoenwelder, M.E.A., 2002. Novel, bioclastic route to self-assembled, 3D, chemically tailored meso/nanostructures: shape-preserving reactive conversion of biosilica (diatom) microshells. *Adv. Mater.* 14 (6), 429–433.
- Schmidt-Rohr, K., Spiess, H.W., 1994. *Multidimensional Solid-state NMR and Polymers*. Academic Press, London.
- Schonberg, C.H.L., 2001. New mechanisms in demosponge spicule formation. *J. Mar. Biol. Assoc. UK* 81, 345–346.
- Schwab, D.W., Shore, R.E., 1971a. Fine structure and composition of a siliceous sponge spicule. *Biol. Bull.* 140, 125–136.
- Schwab, D.W., Shore, R.E., 1971b. Mechanism of internal stratification of siliceous sponge spicules. *Nature* 232, 501–502.
- Shimizu, K., Cha, J.N., Stucky, G.D., Morse, D.E., 1998. Silicatein  $\alpha$ : cathepsin L-like protein in sponge biosilica. *Proc. Natl. Acad. Sci. USA* 95, 6234–6238.
- Shimizu, K., Morse, D.E., 2000. The biological and biomimetic synthesis of silica and other polysiloxanes. In: Bauerlein, E. (Ed.), *Biomaterialization: From Biology to Biotechnology and Medical Application*. Wiley-VCH, Weinheim, pp. 207–219.
- Shore, R.E., 1972. Axial filament of siliceous sponge spicules, its organic components and synthesis. *Biol. Bull.* 143, 125–136.
- Simpson, T.L., Vaccaro, C.A., 1974. Ultrastructural study of silica deposition in freshwater sponge *Spongilla lacustris*. *J. Ultrastruct. Res.* 47, 296–309.
- Simpson, T.L., Volcani, B.E., 1981. *Silicon and Siliceous Structures in Biological Systems*. Springer-Verlag, New York.
- Simpson, T.L., 1984. *The Cell Biology of Sponges*. Springer-Verlag, New York.

- Simpson, T.L., Langenbruch, P.F., Scaleriacci, L., 1985. Silica spicules and axial filaments of the marine sponge *Stelletta grubii* (Porifera, Demospongiae). *Zoomorphology* 105, 375–382.
- Schmid, A.M., Schulz, D., 1979. Wall morphogenesis in diatoms—deposition of silica by cytoplasmic vesicles. *Protoplasma* 100 (3–4), 267–288.
- Sumerel, J.L., Morse, D.E., 2003. Biotechnological advances in biosilicification. In: Müller, W.E. (Ed.), *Prog. Mol. Subcellular Biol.*, vol. 33: Silicon Biomineralization: Biology—Biochemistry—Molecular Biology—Biotechnology. Springer-Verlag, Berlin, pp. 225–247.
- Sumper, M., 2002. A phase separation model for the nanopatterning of diatom biosilica. *Science* 295 (5564), 2430–2433.
- Sundar, V.C., Yablon, A.D., Grazul, J.L., Ilan, M., Aizenberg, J., 2003. Fibre-optical features of a glass sponge—some superior technological secrets have come to light from a deep-sea organism. *Nature* 424 (6951), 899–900.
- Theunissen, J.D., 1994. A method for isolating and preparing silica bodies in grasses for scanning electron microscopy. *Biotechnol. Histochem.* 69, 291–294.
- Uriz, M.J., Turon, X., Becerro, M.A., 2000. Silica deposition in demosponges: spiculogenesis in *Crambe crambe*. *Cell Tissue Res.* 301, 299–309.
- Volcani, B.E., 1981. In: Simpson, T.L., Volcani, B.E. (Eds.), *Silicon and siliceous structures in biological systems*. Springer-Verlag, New York, pp. 157–201.
- Vrieling, E.G., Beelen, T.P.M., van Santen, R.A., Gieskes, W.C., 1999. Diatom silicon biomineralization as an inspirational source of new approaches to silica production. *J. Biotechnol.* 70 (1–3), 39–51.
- Weaver, J.C., Morse, D.E., 2003. Molecular biology of demosponge axial filaments and their roles in biosilicification. *Micro. Res. Tech.* 62 (4), 356–367.
- Wetherbee, R., Crawford, S.A., Mulvaney, P., 2000. The nanostructure and development of diatom biosilica. In: Baeuerlein, E. (Ed.), *Biomineralization: from Biology to Biotechnology and Medical Application*. Wiley-VCH, Weinheim, pp. 189–206.
- Zhou, Y., Shimizu, K., Cha, J.N., Stucky, G.D., Morse, D.E., 1999. Efficient catalysis of polysiloxane synthesis by silicatein alpha requires specific hydroxy and imidazole functionalities. *Angew. Chem. Int. Ed.* 38 (6), 780–782.